

2022

Characterisation of Holographic Recording in Environmentally Stable Photopolymerisable Glass

Tatsiana Mikulchyk

Technological University Dublin, tatsiana.mikulchyk@tudublin.ie

Pamela Stoeva

Technological University Dublin, pamela.stoeva@tudublin.ie

Alicja Kaworek

Technological University Dublin, alicja.kaworek@tudublin.ie

See next page for additional authors

Follow this and additional works at: <https://arrow.tudublin.ie/cieoart>



Part of the [Optometry Commons](#)

Recommended Citation

Mikulchyk, T., Stoeva, P. & Kaworek, A. (2022). Characterisation of Holographic Recording in Environmentally Stable Photopolymerisable Glass. *Applied Science*, vol.12, pg. 5969. <https://doi.org/10.3390/app12125969>

This Article is brought to you for free and open access by the Centre for Industrial and Engineering Optics at ARROW@TU Dublin. It has been accepted for inclusion in Articles by an authorized administrator of ARROW@TU Dublin. For more information, please contact arrow.admin@tudublin.ie, aisling.coyne@tudublin.ie, vera.kilshaw@tudublin.ie.

Funder: This research received no external funding

Authors

Tatsiana Mikulchyk, Pamela Stoeva, Alicja Kaworek, Mohamed Oubaha, Brian Rogers, Suzanne Martin, Dervil Cody, and Izabela Naydenova

Article

Characterisation of Holographic Recording in Environmentally Stable Photopolymerisable Glass

Tatsiana Mikulchyk ^{1,*} , Pamela Stoeva ¹, Alicja Kaworek ², Mohamed Oubaha ², Brian Rogers ¹, Suzanne Martin ¹, Dervil Cody ¹  and Izabela Naydenova ¹ 

¹ Centre for Industrial and Engineering Optics, School of Physics and Clinical & Optometric Sciences, College of Sciences and Health, Technological University Dublin, D07 EWV4 Dublin, Ireland; c15335981@mytudublin.ie (P.S.); c14507363@tudublin.ie (B.R.); suzanne.martin@tudublin.ie (S.M.); dervil.cody@tudublin.ie (D.C.); izabela.naydenova@tudublin.ie (I.N.)

² Centre for Research in Engineering Surface Technology, Technological University Dublin, D08 NF82 Dublin, Ireland; alicekaworek@gmail.com (A.K.); am.oubaha@gmail.com (M.O.)

* Correspondence: tmikulchyk@gmail.com

Featured Application: Development of holographic optical elements with controlled diffraction efficiency and improved environmental stability in water-resistant photopolymerisable hybrid sol-gel material.

Abstract: Photopolymerisable glasses are holographic recording materials which provide good recording capability, improved dimensional stability, and negligible shrinkage. Recently, a novel photopolymerisable hybrid sol-gel (PHSG) for holographic recording of volume gratings has been reported. The PHSG has significantly improved gelation time and high water resistance, both of which make it an attractive material for mass production of holographic optical elements (HOEs) with no sensitivity to ambient humidity. In order to achieve full control over the performance of the material and further improve its properties, a study of grating formation under holographic patterning is essential. This paper reports characterisation of the grating recording in PHSG. The approach is based on the analysis of grating parameters during exposure and post-recording dark processes. The obtained results suggest that photopolymerisation of the methacrylate groups is the main contributor to the creation of refractive index modulation during exposure. During the dark process, the enhancement of the refractive index modulation is observed, probably due to further polycondensation. The observations made facilitate controlled and predictable diffraction efficiency of gratings recorded on the PHSG, thereby furthering the prospect of the development of HOEs with customisable specification.

Keywords: photopolymerisable glass; volume holography; holographic recording material; water-resistant material; sol-gel chemistry; holographic optical element



Citation: Mikulchyk, T.; Stoeva, P.; Kaworek, A.; Oubaha, M.; Rogers, B.; Martin, S.; Cody, D.; Naydenova, I. Characterisation of Holographic Recording in Environmentally Stable Photopolymerisable Glass. *Appl. Sci.* **2022**, *12*, 5969. <https://doi.org/10.3390/app12125969>

Academic Editor: Andrés Márquez

Received: 16 May 2022

Accepted: 9 June 2022

Published: 11 June 2022

Publisher's Note: MDPI stays neutral with regard to jurisdictional claims in published maps and institutional affiliations.



Copyright: © 2022 by the authors. Licensee MDPI, Basel, Switzerland. This article is an open access article distributed under the terms and conditions of the Creative Commons Attribution (CC BY) license (<https://creativecommons.org/licenses/by/4.0/>).

1. Introduction

The interest in new holographic recording materials with significantly improved durability and environmental stability and/or additional functionality [1,2] is driven by rapid development of Augmented Reality displays [3–5], sustainable and energy-saving LED lighting [6,7], and solar energy collection technology [8,9]. As shown previously, any variations of the diffraction efficiency, the diffraction angle, and/or the diffraction spectrum cause undesirable effects on the device performance [5]. Thus, resistance of the holographic recording material to the environment provides stable performance of HOEs at different environmental conditions and ensures their successful implementations in real-world products.

Photopolymerisable glasses as holographic recording materials are good candidates due to their high recording capability [10,11], improved dimensional stability [12], and

negligible shrinkage [13]. In addition, photopolymerisable glasses overcome the thickness limitations inherent to holographic photopolymers and allow achieving high density recording [11]. Recently, a novel photopolymerisable hybrid sol-gel (PHSG) for holographic recording of both transmission and reflection volume gratings with refractive index modulation up to 3×10^{-3} has been reported [14]. The PHSG has significantly improved gelation time in comparison with other photopolymerisable glasses and high water resistance, both of which make it an attractive material for mass production of HOEs with no sensitivity to ambient humidity.

In order to achieve full control over the performance of the material and further improve its properties, understanding of the processes of grating formation under holographic patterning is essential. Research on the mechanism of grating formation has been recently reported for a Class I photopolymerisable hybrid organic-inorganic material [15]. The material consists of a silicate sol-gel matrix that incorporates organic monomers, inorganic high refractive index species, and a photoinitiator. According to classification based on the nature of the links between the inorganic and organic components, Class I represents systems with no covalent bonds between the organic and inorganic species [16]. As found in [15], the grating formation involves two stages: exposure and dark processes. During exposure, photopolymerisation occurs in illuminated areas leading to the refractive index modulation and, as a result, grating formation. Further enhancement of the refractive index modulation is observed in darkness, and it is attributed to the diffusion of two components: monomers and high refractive index species [15]. Diffusion of mobile components in Class I photopolymerisable glasses is feasible due to the absence of covalent bonds between the sol-gel matrix and polymerisable (monomers) and diffusible (photoinitiator, dopants) species.

This paper focuses on the investigation of the mechanism of grating formation in a recently developed PHSG. Similarly to the above-mentioned research, the approach is based on the analysis of grating parameters during exposure and post-recording dark processes. It should be noted that this PHSG has a principal difference in its structure, as it is the first example of a Class II photopolymerisable glass where the organic and inorganic components have strong chemical bonds [16]. Thus, it is expected that the difference in the structure of Class I and Class II materials may lead to the domination of different processes during exposure and post-recording dark process.

Along with a study of grating formation, this paper reports on the investigation of other aspects of the PHSG which have an effect on the performance of the HOEs. This includes the aging effect of the sol on the holographic recording capability of PHSG and its sensitivity to temperature and environmental humidity. Good understanding and control of these parameters will allow the development of HOEs based on PHSG with predictable diffraction efficiency and sustainable performance at different environmental conditions.

2. Materials and Methods

2.1. Preparation of PHSG

Detailed description of the PHSG development was reported in [14]. Briefly, the PHSG was synthesised by employing a four-step sol-gel process using two hybrid precursors: 3-trimethoxysilylpropyl methacrylate (MAPTMS, purchased from Safic-Alcan) and a zirconium complex (ZCO) prepared from the chelation of zirconium (IV) propoxide (ZPO, purchased from Merck) and methacrylic acid (MAA, purchased from Merck). The first step involved the formation of the hybrid silicate matrix and the complexation of the transition metal. Therefore, MAPTMS (6.04×10^{-2} mol) was mixed with HNO_3 (4.44×10^{-2} mol) for 45 min. Simultaneously, in a separate container, ZPO (2.218×10^{-3} mol) was complexed by MAA (1.567×10^{-3} mol) and enabled to react for 45 min to form the ZCO complex. In the second step, the two hybrid components (hybrid silicate and ZCO solutions) were mixed together and left to stir for 10 min to enable the formation of a transparent and homogeneous sol. The third step included a second hydrolysis performed with deionized water (6.04×10^{-2} mol) leading to an optimum total hydrolysis rate of 55% (against the

total alkoxide groups). The sol was then left to stir at ambient temperature for 24 h to enable the completion of the sol-gel reactions. At the fourth step, in order to increase the condensation ability of the hybrid nanoparticles, modification of the sol-gel was carried out by adding (3-aminopropyl)triethoxysilane (APTES, purchased from Merck) in a content of 3.608×10^{-3} mol. Along with APTES, a photoinitiator, Bis(eta.5-2,4-cyclopentadien-1-yl)-bis(2,6-difluoro-3-(1H-pyrrol-1-yl)-phenyl) titanium (Irgacure 784, purchased from Ciba) was added in a content of 1.81×10^{-4} mol in order to make the material photosensitive. After another 10 h of stirring, the full reaction of APTES with the hybrid sol-gel matrix was completed. UV-Vis absorption spectrum of the sol dissolved in isopropanol showed a wide absorption band with the peak absorbance at 480 nm [14].

2.2. Dynamic Light Scattering (DLS)

DLS analysis was used for characterisation of the particle size distribution of the sol-gel material in colloidal form using a Malvern Nano-ZS instrument. The sample for the test was prepared by diluting the sol with 2-propanol using the ratio 1:4 and then filtered using a filter with 1 μm porosity. The experiments were conducted at ambient temperature. The aging of the sol for up to 30 days was tested.

2.3. Layer Preparation

Thin layers were prepared by a drop casting method on the levelled glass slide ($75 \times 25 \text{ mm}^2$, 1 mm thickness). To coat the glass slide, solution was released from a single channel graduated pipette and simultaneously distributed over the entire surface area of the glass slide. After coating, the samples were cured at 125 $^{\circ}\text{C}$ for 45 min in the oven (Binder, model ED56) to remove the liquid phase from the gel and develop dry nanoporous glass layers suitable for holographic recording. After drying, the layers prepared with 0.30 and 0.45 mL of sol had thickness of 88 ± 2 and $118 \pm 3 \mu\text{m}$, respectively.

2.4. Holographic Recording and Grating Thickness Estimation

Holographic recording of volume phase transmission gratings was carried out by exposing the PHSG layer to two beams of 532 nm wavelength from a Nd:YVO₄ laser (Coherent, model Verdi) as shown in Figure 1. The recording beam had a diameter of 6 mm, allowing the development of a grating with the area of about 1.13 cm². The angle of incidence of the recording beams (θ) was 12.3 $^{\circ}$ with respect to the normal to the surface of the sample. This recording geometry provided an unslanted grating with spatial frequency of approximately 800 lines mm⁻¹. The optimum total recording intensity of 20 mW cm⁻² was used. The exposure time was varied depending on the aim of the experiment; more details on recording conditions are provided in Section 3. For the real-time diffraction efficiency growth curve recording and Bragg selectivity curve measurements, a low intensity (1.8 mW cm⁻²) 633 nm beam from a He-Ne laser was employed as a probe beam. The laser beam intensity was monitored using an optical power meter (Newport, model 843-R) and the acquired data were transferred to a computer. The position of the sample was computer controlled via a motion controller (Newport ESP300). The diffraction efficiency of the transmission gratings was calculated as the ratio of the first-order diffracted beam intensity and incident beam intensity. The effect of Fresnel reflection on the diffraction efficiency value was taken into account by measuring the intensity of the incident probe beam after the unexposed layer.

Transmission gratings with the thickness of about 88 and 118 μm can be considered as volume gratings as the Klein-Cook Q-parameter [17] is found to be 126 and 169, respectively. Quantitative analysis of recorded gratings was carried out using a coupled-wave theory [18] and the thickness (d) of the grating was estimated from the experimental Bragg angular selectivity curves utilising the following equation:

$$\Delta\theta_{\text{FWHM}} = \frac{\Lambda}{d} \quad (1)$$

where $\Delta\theta_{FWHM}$ is the full angular bandwidths at the half of the maximum of the diffraction efficiency and Λ is the spatial period.

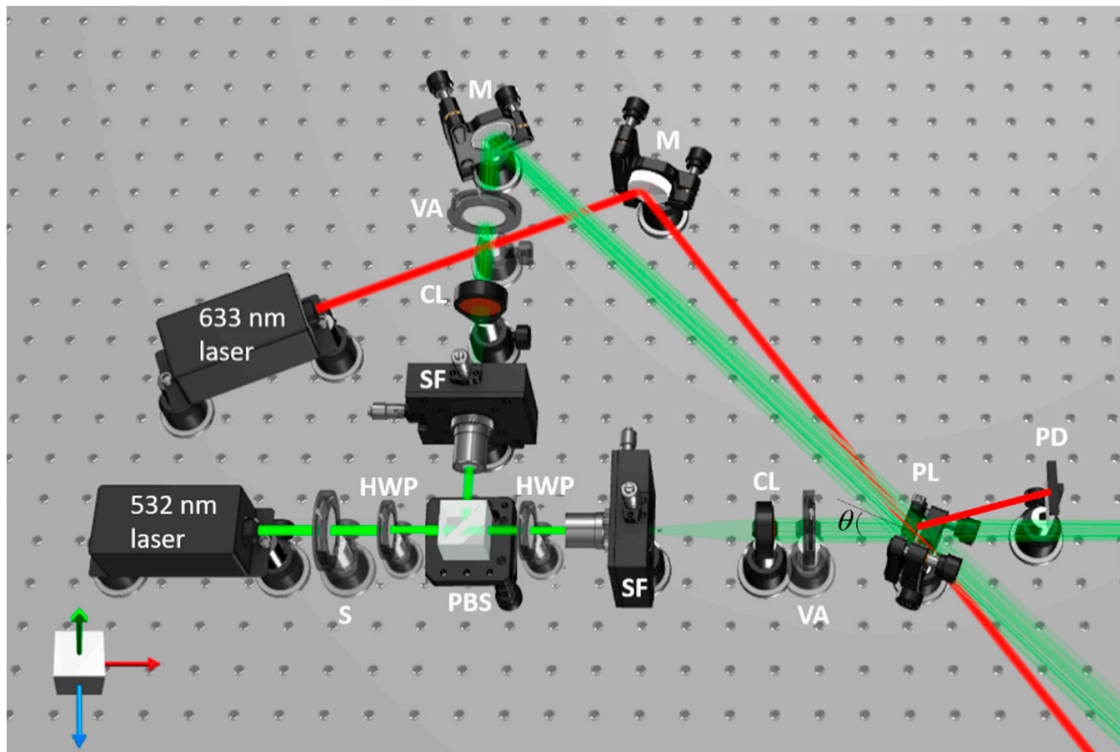


Figure 1. Experimental set-up for holographic recording of transmission gratings using a 532 nm laser. Monitoring of the diffraction efficiency growth curve is performed by probing with a 633 nm laser and collecting beam intensity data with a photodetector positioned at the diffracted beam path. S—electronic shutter, HWP—half-wave plate, PBS—polarising beam splitter, SF—spatial filter, CL—collimator, VA—variable aperture, PL—PHSG layer, M—mirror, PD—photodetector.

2.5. Pendulum Hardness Test

Pendulum hardness testing allows characterising the hardness of the surface of the material. Standard hardness tests relate oscillation damping to surface hardness. The higher the number of oscillations, the higher the surface hardness. The surface hardness of PHSG layers was characterised using the Sheen Instruments Ltd. Pendulum Hardness Tester type 707KP.

The $88 \pm 2 \mu\text{m}$ layers were prepared using the sol immediately after completing the synthesis or with age of 0-day. To simulate bright fringe areas, the layers were exposed to uniform 532 nm laser beam with an intensity of 40 mW cm^{-2} . The value of 40 mW cm^{-2} was used in order to achieve the degree of polymerisation corresponding to that in the bright fringe areas obtained during holographic recording with the total recording intensity of 20 mW cm^{-2} . Exposure times from 20 to 160 s were used.

The surface hardness of an unexposed sample and samples exposed to the uniform beam was measured using the König test. The König test for hard coatings measures the time taken for the amplitude to decrease from 6° to 3° and evaluates the number of oscillations which occurred. The test was performed during the time period from 5 min to 24 h after exposure with the aim to estimate the evolution of the surface hardness with time.

3. Results and Discussion

3.1. Aging of the Sol

The developed sol, as described in Section 2.1, represents a stable dispersion of colloidal amorphous particles in an alcoholic solvent (composed of methanol and propanol).

The sol particles may interact by van der Waals forces or hydrogen bonds leading to their agglomeration and as a result higher viscosity of the sol that affects sol coatability and the morphology of the final coatings [19,20]. As the layer uniformity is one of the crucial parameters required for recording of HOEs with sustainable performance, the optimal age of the sol for achieving uniform layers needs to be identified. In this study, the aging effect of the sol is systematically investigated in terms of the size and homogeneity of the sol particles and viscosity of the sol.

Characterisation of the size of nanoparticles composing the sol with age up to 30 days was carried out by means of DLS analysis. A monomodal distribution curve with a peak of intensity of approximately 4.5 nm was obtained for the sol immediately after completing the synthesis (Figure 2a). An increase of the average nanoparticle size was observed with time, reaching 10.7 and 13.5 nm after 15 and 30 days, respectively (Figure 2b). To define the dispersion of nanoparticles, the full width at half maximum of the size distribution (Figure 2a) was calculated. This was found to be 4.2, 23.3, and 30.3 nm for the sol with the age of 0, 15, and 30 days, respectively. These data demonstrate that one of the main effects of sol aging was agglomeration of particles and higher dispersion of nanoparticle population.

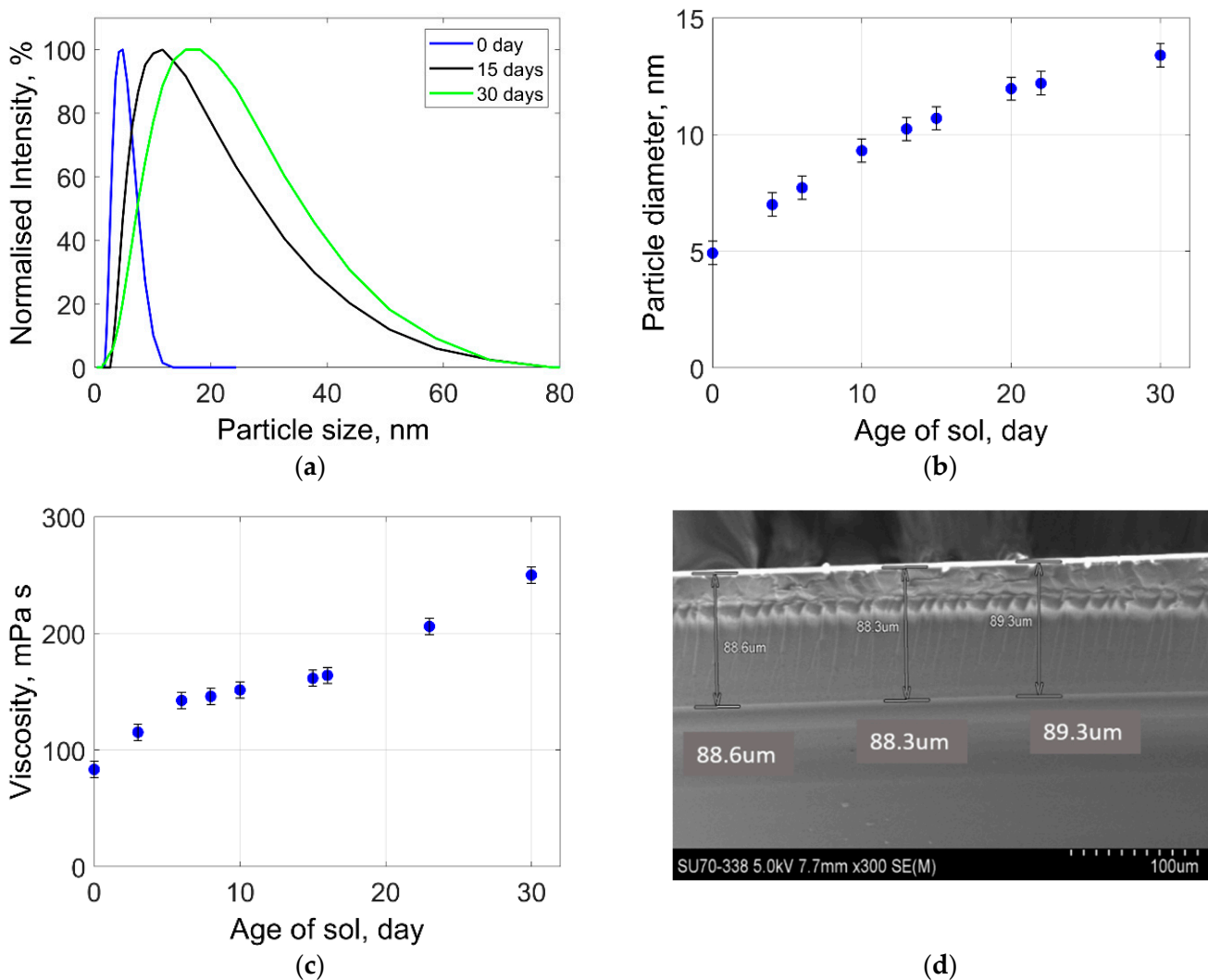


Figure 2. (a) Particle size distribution of the sol with age of 0, 15, and 30 days obtained by DLS analysis; (b) particle size diameter of the sol obtained from the peak of intensity of the size distribution curve (Figure 2a) versus the age of the sol; (c) dynamic viscosity of the sol with different age; (d) SEM image of the cross-section of PHSG layer prepared by use of sol with age of 7 days.

Simultaneously with DLS analysis, the dynamic viscosity of the sol was measured in order to identify the limit period when the sol could produce uniform thick layers. Dynamic viscosity was determined by means of an AND Viscometer (SV-10). As expected, growth in nanoparticle size caused the substantial increase of dynamic viscosity from 85 to 250 mPa s within 30 days (Figure 2c). Experimental results showed that the sol with dynamic viscosity of up to 250 mPa s, corresponding to an age of up to 30 days, was suitable for coating. The layer homogeneity and thickness was then investigated by imaging a cross-section of samples via SEM. SEM images were recorded by means of a Hitachi SU-70 SEM using an accelerating voltage of 5 keV. Three measurements were done at different points to evaluate the thickness uniformity. It was found that layers prepared with sol aged up to 7 days had homogenous coatings with thicknesses of $88.8 \pm 0.5 \mu\text{m}$ (Figure 2d). More aged sol led to non-uniformity of the coating, with thickness variation reaching up to $15 \mu\text{m}$ within the glass slide area. Thus, it was proposed that the sol age of up to 7 days could be considered as the optimum for obtaining layers with uniform thickness. The effect of the sol age on the holographic recording capability was also investigated and the results are presented in the section below.

3.2. Effect of the Sol Age on Holographic Recording Capability

The effect of the sol age on the holographic recording capability was investigated by recording volume phase transmission gratings. Two batches containing ten layers ($118 \pm 3 \mu\text{m}$ thickness) were prepared using the sol with ages of 0 and 7 days at the time of exposure. To analyse the grating formation in PHSG and estimate its photosensitivity, diffraction efficiency growth curves were monitored in real time during exposure. Figure 3a gives a representative example of the growth curves for two layers with the same thickness ($118 \mu\text{m}$) but prepared using the sol with different ages (0 and 7 days). The typical diffraction efficiency growth started after 8 s of exposure. This 8 s period was attributed to the oxygen inhibition inherent to photoinduced polymerisation of methacrylates [21]. After 35 s exposure, the diffraction efficiencies of 23 and 18% were achieved in layers prepared using the sol with age of 0 and 7 days, respectively (Figure 3a).

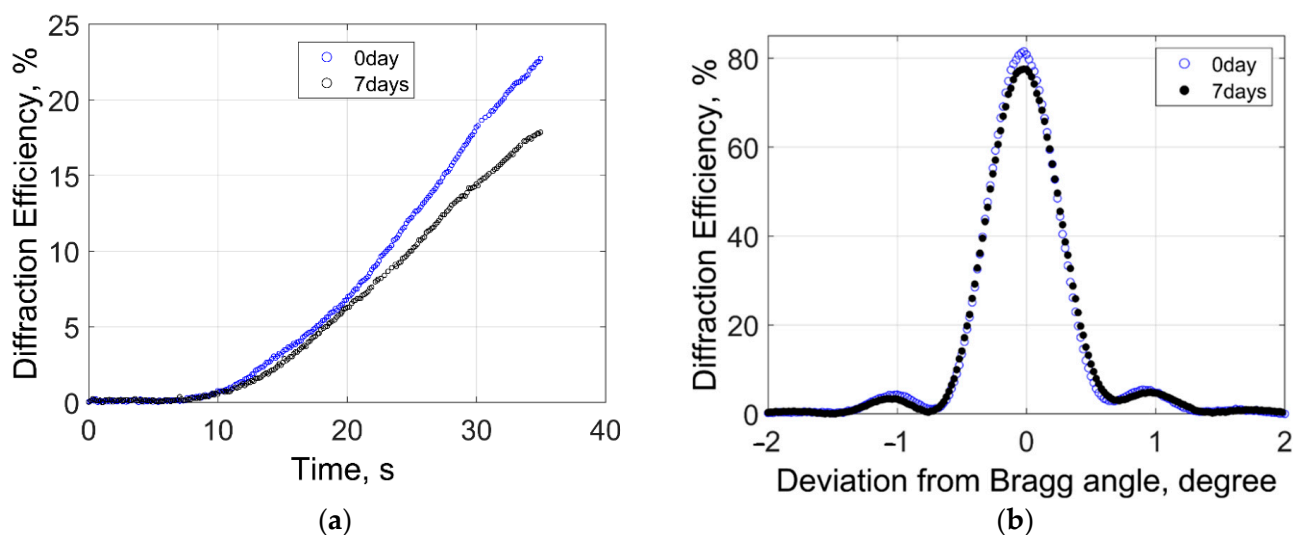


Figure 3. Cont.

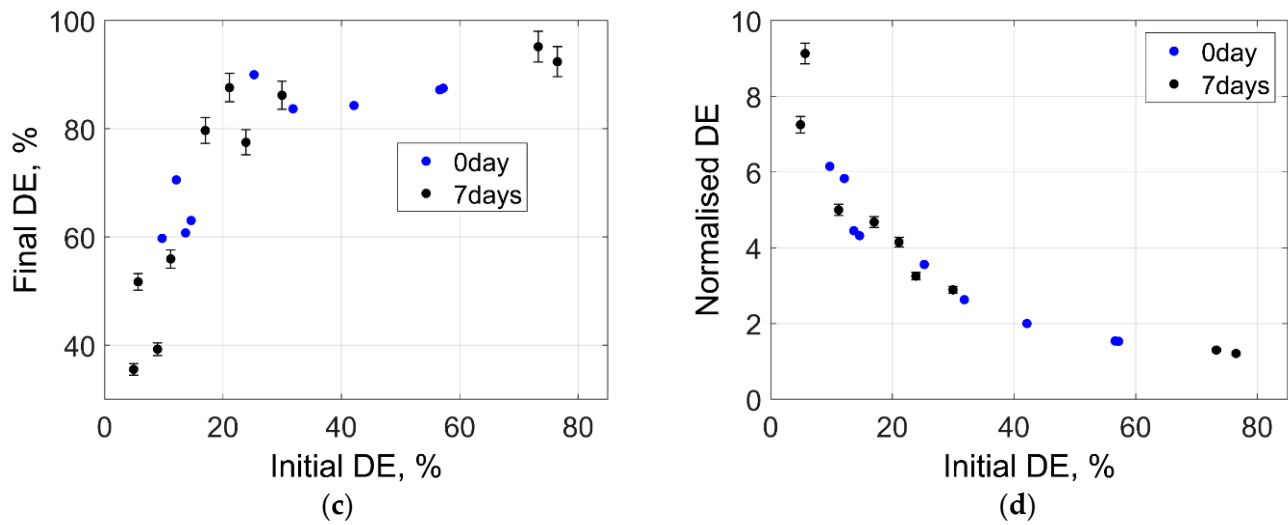


Figure 3. (a) Real-time diffraction efficiency growth during holographic recording on PHSG layers with thickness of 118 μm prepared using the sol with ages of 0 and 7 days; (b) Bragg selectivity curves of gratings recorded as shown on Figure 3a and measured in 24 h after recording; (c) final diffraction efficiency (DE) measured 24 h after exposure versus the initial diffraction efficiency obtained during exposure; (d) normalised DE versus initial DE shows the level of the enhancement during dark process.

Photosensitivity (S) was defined as the ratio between the square root of the diffraction efficiency and the product of the total recording intensity (I), exposure time (t), and the visibility (V) [22]:

$$\sqrt{\eta} = SIVt \quad (2)$$

where visibility was defined as

$$V = \frac{2R^{-1/2}}{(1 + R)} \quad (3)$$

where R is the ratio of the recording beam intensities. In the current experimental conditions, the holographic recording was performed using two beams with equal intensity which provided $R = 1$. As a result, photosensitivity of layers prepared using the sol with ages of 0 and 7 days was found to be 8×10^{-4} and $7 \times 10^{-4} \text{ mJ}^{-1} \text{ cm}^2$, respectively. Thus, an approximate 14% decrease of photosensitivity was observed within 7 days and, hence, the longer exposure was needed to achieve the required diffraction efficiency. Photosensitivity is directly linked to the polymerisation rate, which is highly dependent on the capability of the photoinitiator to produce free radicals [16]. Therefore, the observed photosensitivity decrease could be explained by photodegradation of a photoinitiator that might lead to the loss of the photochemical reactivity of the formulation as previously reported for similar hybrid material [23].

The diffraction efficiency was measured again 24 h after recording and an increase up to 81.5% (0-day) and 77.5% (7-days) was observed (Figure 3b). This indicated that further enhancement of the diffraction efficiency occurred during a dark process. It was found that the level of enhancement of the diffraction efficiency depended on the initial diffraction efficiency achieved after exposure and followed the same trend for samples prepared using sol of 0 and 7 days (Figure 3c). Normalized diffraction efficiency calculated as the ratio of the diffraction efficiency measured 24 h after recording and immediately after recording was used to estimate the diffraction efficiency enhancement level (Figure 3d). As seen from Figure 3d, the gratings with initial diffraction efficiency of about 10% achieved after exposure showed diffraction efficiency enhancement up to 6-fold, which corresponded to about 60% diffraction efficiency measured 24 h after exposure. Three days after exposure, the diffraction efficiency was measured again, and no further increase of the diffraction

efficiency was noticed for all samples. Thus, the dark process is supposed to be completed within 24 h after exposure. The mechanism of this significant dark process was investigated further and results are presented in Section 3.3.

3.3. Holographic Grating Formation

The fundamental motivation for investigation of the grating formation process is to obtain predictable diffraction efficiency and to control holographic recording capability by modifying the composition. As a result, this allows the development of HOEs with customisable specification and the addition of practical advantage in terms of their sustainable performance.

In order to identify mechanisms contributing to the grating formation in PHSG, diffraction efficiency was monitored during holographic recording (exposure) and after recording (dark process when laser is off). This approach allowed studying the impact of both physicochemical reactions and physicochemical processes on the refractive index modulation formation during exposure and dark processes.

Volume phase transmission gratings were recorded using the set-up presented in Figure 1. Layers with thickness of $118 \pm 3 \mu\text{m}$ were prepared using the sol with the age of 0-day as described in Section 2.3. Figure 4a shows the typical real-time diffraction efficiency growth curves of gratings obtained using exposure times of 25, 30, and 35 s. As seen from Figure 4a, during exposure the growth curves for 25, 30, and 35 s recording time had the same trend and diffraction efficiencies of 14.7, 20.1, and 25.2% were reached, respectively. At this stage, the key photochemical reaction is likely to be the photopolymerisation of the methacrylate groups (MAPTMS and MAA), leading to the formation of rigidly structured nanoparticle-based species in the bright fringe areas resulting in the creation of a diffraction grating [14].

Previous research on grating formation in Class I materials shows that diffusion of photoinitiator molecules and monomers due to the concentration gradient between bright and dark regions created during exposure also plays a part in grating formation [15]. These materials represent diffusing host-guest systems where the contribution of diffusion to the final diffraction efficiency is significant. The PHSG described here is a Class II material and, thus, has a principally different structure that may affect diffusion in the volume of the material.

The sol-gel process employed for PHSG development (as described in Section 2.1) enables the fabrication of nanoparticles from small hybrid molecules. In this process, all small molecules reacted via hydrolysis and condensation reactions to form oligomeric microporous silicate-based nanoparticle systems, as demonstrated by Si-NMR spectroscopy in closely related material systems [24]. Therefore, as a result of thermal curing, the PHSG can be represented as an interconnected network of microporous hybrid silicate and zirconium oxide nanoparticles, where photoinitiator molecules would be able to diffuse and further enable photoreaction processes. Thus, during exposure, photopolymerisation is expected to be the main contributor to the grating formation. Diffusion of photoinitiator may also contribute to some extent but previous work has shown that these diffusion effects are likely to be limited due to low permeability of the material [14]. The systematic study, involving the recording of structures with largely different spatial frequencies, of the diffusion effects in PHSG will be the scope of future research.

After exposure, the diffraction efficiency was monitored for 25 min in dark and its increase up to 78.2, 79.5, and 79.1% was observed for gratings with the exposure of 25, 30, and 35 s, respectively (Figure 4b). These results showed that the final diffraction efficiency of gratings recorded on the layers with same thickness did not depend, in this instance, on the initial exposure. This is evidence that once grating growth is in progress, the influence of processes unrelated to the exposing interference pattern is significant. These 'dark' processes become the dominant grating growth process and continue for about 24 h leading to the increase of the diffraction efficiency (Figure 3c). After 24 h, no further increase of the

diffraction efficiency is observed and, as shown previously in [14], its stability has been confirmed for 27 months.

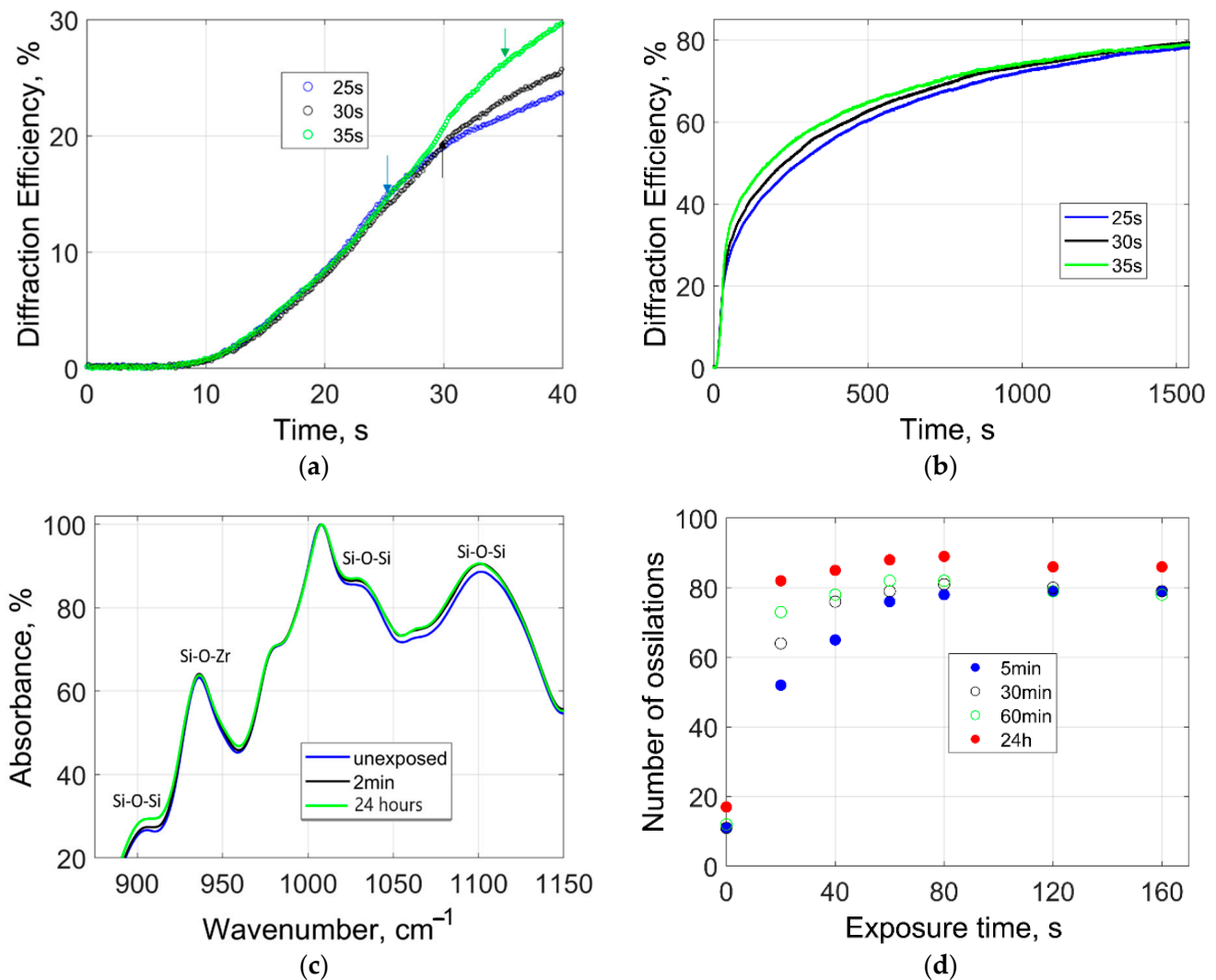


Figure 4. (a) Real time diffraction efficiency growth curves of transmission gratings monitored during holographic exposure for 25, 30, and 35 s; arrows show the end of laser exposure; (b) diffraction efficiency growth curves of samples shown in Figure 4a monitored during both holographic recording and dark process for 25 min; (c) FTIR spectra of PHSG layers measured before exposure to 532 nm uniform beam and 2 min and 24 h after exposure (during dark process); (d) hardness test results (number of oscillations) for layers exposed to uniform beam for 20 to 160 s show that within 24 h the layers reach similar hardness.

To identify the origin of the dark process, FTIR spectra (obtained using a Perkin Elmer GX instrument) of the PHSG layers before and after exposure were compared (Figure 4c). This approach allows mimicking of the dark and bright fringe areas of the grating and analysing changes induced by exposure. For this experiment, the layers were exposed to a uniform 532 nm wavelength beam with the intensity of 40 mW cm^{-2} for 20 s. FTIR spectra were obtained before exposure and 2 min and 24 h after exposure (Figure 4c). It can be seen that following the exposure, the siloxane (900 , 1030 , and 1100 cm^{-1}) and silicon-zirconium oxide (930 cm^{-1}) bands constituting the inorganic network of the hybrid sol-gel material are increased, confirming the enhancement of the condensation of the material. This can only be explained by the occurrence of polycondensation reactions between the residual unreacted silanol and zirconium hydroxide groups, forming more condensed and robust

inorganic chemical bonds. Interestingly, this pure inorganic polycondensation process has been enabled by the radical organic polymerisation reactions, which increased proximity between the inorganic reactive sites. Therefore, the dominant effect on the grating formation during the dark process is proposed to be the inorganic polycondensation process which causes an increase of the density in bright fringe areas, leading to the higher refractive index contrast and as a result the diffraction efficiency enhancement.

This concept is further supported by the hardness testing data of polymerised layers as shown in Figure 4d. In this experiment, layers were exposed to a uniform laser beam with the intensity of 40 mW cm^{-2} for 20 to 160 s, to induce different extents of initial polymerisation. Hardness testing was then performed within 24 h to identify the changes in hardness caused by the dark process. As seen from Figure 4d, after exposure the layers illuminated for 20 to 160 s showed oscillation number from 52 to 80, respectively. After 24 h, these layers reached similar robustness and the oscillation number was in the range from 82 to 89. This increase in hardness supports the hypothesis that the dark process occurring after recording can be attributed to further polycondensation, leading to lower pore diameters and microporosity [25,26].

3.4. Fixation of Holographic Grating by UV-Curing

In many instances, it may be preferable to prevent the effect of the dark process on the refractive index modulation and to fix the diffraction efficiency at the level obtained after exposure. The suitability of UV-curing for this purpose was studied. For this experiment, transmission gratings were recorded using exposure time of 15, 30, 45, and 60 s by means of the set-up presented in Figure 1. The diffraction efficiency was monitored immediately after exposure and it was found to reach up 85% (60 s exposure time) in layers with thickness of about $120 \mu\text{m}$. Then, the samples were exposed to UVA light by means of a Dymax UV-curing System (ECE Series) for 297 s with 29 mW cm^{-2} intensity and the diffraction efficiency was measured again.

The effect of UV-curing was analysed by calculating the normalised diffraction efficiency as the ratio of the diffraction efficiency obtained after UV-curing and after exposure (Figure 5a). As seen from Figure 5a, the decrease of diffraction efficiency of 7 and 16% was obtained for gratings recorded with the exposure time of 30 and 15 s, respectively. Longer exposures (45 and 60 s) provided an increase of the diffraction efficiency for few percent and allowed fixing the diffraction efficiency at the level that was close to that achieved during holographic recording. For example, the grating with 85% diffraction efficiency measured after recording had 87% after UV-curing.

The stability of the diffraction efficiency after UV-curing was verified by further monitoring the diffraction efficiency for 6 days. Bragg selectivity curves for the typical grating recorded using 30 s exposure time are presented in Figure 5b. As seen from Figure 5b, the diffraction efficiency decreases from 59% (obtained after recording) to 52% after UV-curing. Within 24 h, the diffraction efficiency enhanced just for few percent (up to 56%) and then remained unchanged. Thus, UV-curing was confirmed as an effective approach to prevent enhancement of the refractive index modulation observed during the subsequent dark process as described in Section 3.3. Here, it should be noted that after UV-curing cracking of some layers with thickness above $100 \mu\text{m}$ was noticed. To avoid layer cracking, further optimisation of the layer preparation method is required which might include dilution of the sol with solvents. This will be the scope of future research.

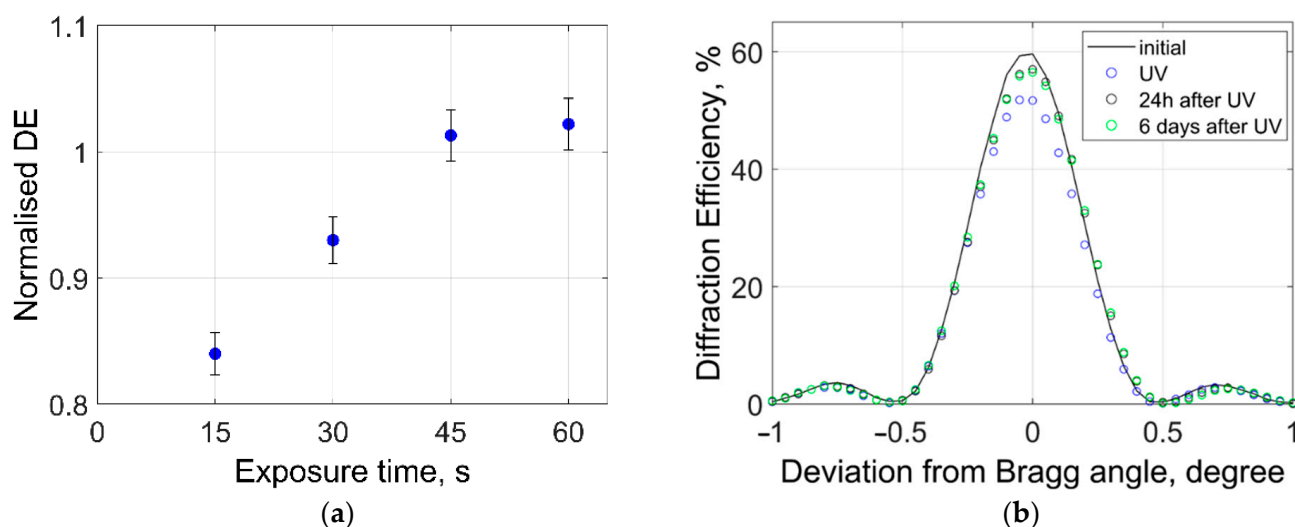


Figure 5. (a) Normalised diffraction efficiency (DE) versus the exposure (recording) time shows the effect of UV-curing on the grating fixation. Normalised diffraction efficiency was calculated as the ratio of the diffraction efficiency obtained after UV-curing and after recording; (b) Bragg selectivity curves of the transmission grating recorded using 30 s exposure demonstrate stability of the diffraction efficiency after UV-curing.

3.5. Environmental Stability

In the current research, the impact of the environmental humidity and temperature on grating stability was investigated by monitoring the diffraction efficiency of transmission gratings at relative humidity up to 95% and temperature of 130 °C, respectively. For the humidity test, the sample was placed in a controlled environment chamber (Electro-tech system, Perkasi, PA, USA, model LV 202-E) as shown in Figure 6a. Diffraction efficiency was measured before humidity exposure at ambient humidity of 50% and temperature of 21 °C (Figure 6b). Then, the humidity level was increased to 70% and the temperature was kept constant at 21 ± 0.3 °C. After 60 min, the sample was removed from the chamber and its Bragg selectivity curve was measured by probing with a 633 nm laser at different incident angles. The same experiment was repeated at 95% RH. As seen from Figure 6b, no changes in either the absolute value of the diffraction efficiency or the profile of the Bragg selectivity curve were observed. This confirms the insensitivity of the PHSG to humidity and broadens the range of its potential applications for the development of holographic optical elements with improved stability at different humidity levels.

For the thermal response test, the layers were coated on a flexible polycarbonate substrate (Bayer Makrofol DE1-1cc, 375 μm thick). The choice of the substrate was governed by the requirements for roll-to-roll manufacturing and integrated optical components considered as the most feasible approach for mass manufacturing of holographic optical components [27]. The temperature resistance of the PHSG was investigated by monitoring the diffraction efficiency of transmission gratings before and after curing in the oven (Binder, model ED56) at 130 °C for 60 min (Figure 6c). Both the diffraction efficiency and the profile of the Bragg selectivity curve were unchanged after exposure to 130 °C. In addition, no defects and cracks were observed on the layer (Figure 6d) and the grating produced a highly efficient diffraction pattern (Figure 6e). These experimental results confirm the resistance of PHSG to high temperature and the capability of holographic optical elements recorded on PHSG to withstand temperatures up to 130 °C.

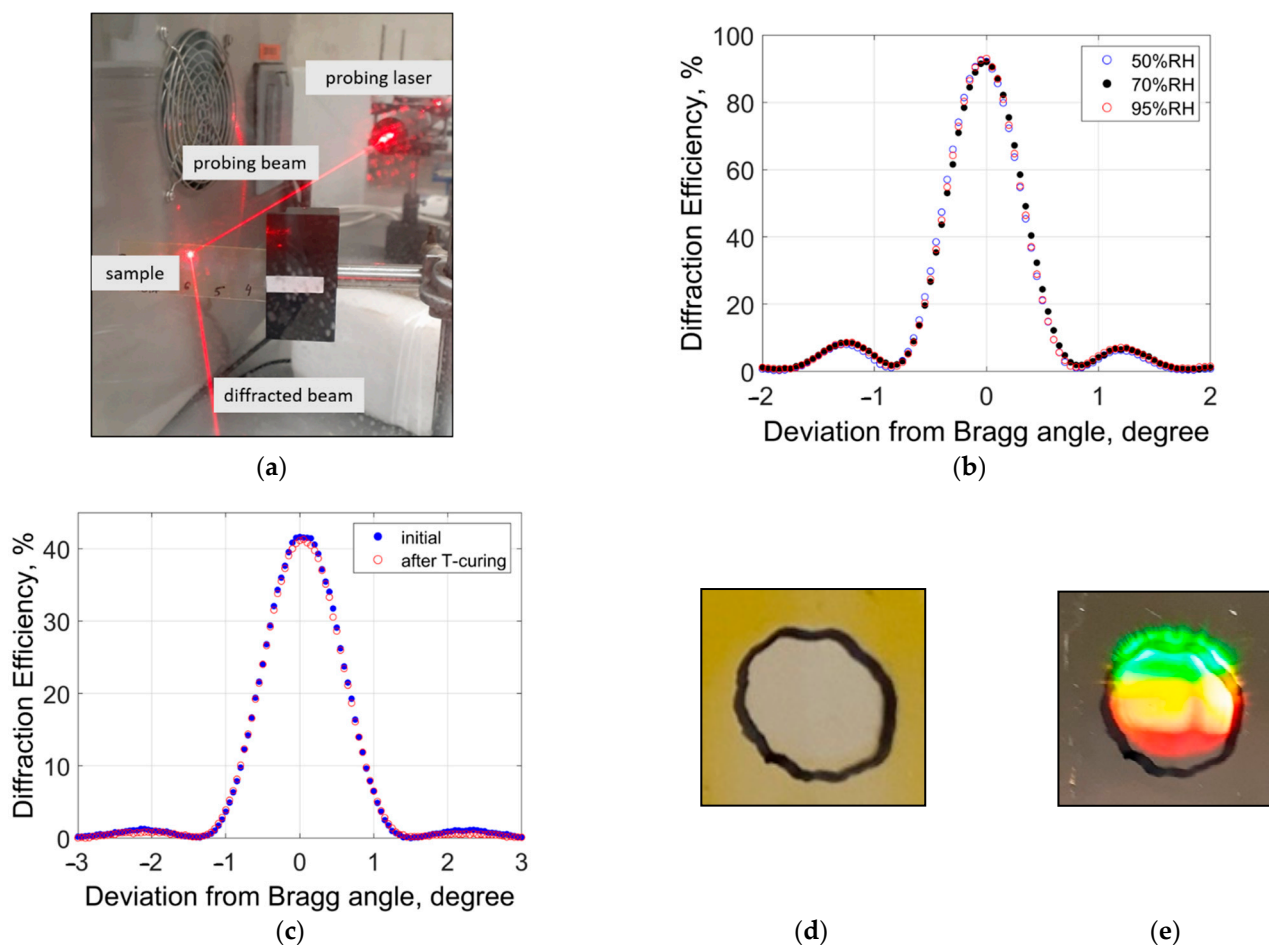


Figure 6. (a) Photograph of the experimental set-up for monitoring the impact of humidity on the diffraction efficiency of transmission gratings recorded on PHSG layers; (b) Bragg selectivity curves of the transmission grating at different levels of relative humidity; (c) Bragg selectivity curves of the transmission grating measured before and after curing at 130 °C for 60 min; (d) Photograph of the PHSG layer after curing at 130 °C for 60 min where the clear part corresponds to the area of the grating; (e) image of the grating (same sample as shown in Figure 3d) under ambient light illumination after curing at 130 °C for 60 min.

4. Conclusions

The process of grating formation in a recently developed photopolymerisable glass (PHSG) was investigated. It was found that the grating formation had two stages: exposure to laser light and post-recording dark processes. During exposure, photopolymerisation of the methacrylate groups was likely to be the main contributor to refractive index modulation formation. During the dark process, further enhancement of the diffraction efficiency was detected. This was attributed to the inorganic polycondensation process which is thought to have the dominant effect on the grating formation at this stage.

Enhancement of the diffraction efficiency during the dark process was found to be dependent on the initial diffraction efficiency achieved after exposure and reached a 6-fold increase. This trend was observed for samples prepared using sol aged for 0 and 7 days. To prevent dark enhancement of the diffraction efficiency and fix the grating, UV-curing was successfully applied.

Thus, highly efficient gratings (up to 90%) can be developed in 118 μm thick PHSG layers prepared with the sol aged up to 7 days. The obtained 6-fold increase of the diffraction efficiency during the dark process is beneficial as it allows for the achievement of high diffraction efficiency by using low exposure. In applications where the precise diffraction

efficiency is necessary, the final diffraction efficiency can be controlled by utilising an appropriate exposure and subsequently UV-curing. Insensitivity of the PHSG to humidity (up to 95%) and temperature (up to 130 °C) broadens the range of potential applications of PHSG for the development of holographic optical elements with improved stability at different environmental conditions.

Author Contributions: Conceptualization, T.M., S.M. and I.N.; methodology, T.M., B.R., P.S., M.O. and A.K.; validation, T.M., P.S., A.K. and B.R.; formal analysis, T.M. and M.O.; investigation, T.M., B.R., P.S. and M.O.; writing—original draft preparation, T.M., M.O., D.C., S.M. and I.N.; writing—review and editing, T.M., D.C. and I.N. All authors have read and agreed to the published version of the manuscript.

Funding: This research received no external funding.

Institutional Review Board Statement: Not applicable.

Informed Consent Statement: Not applicable.

Data Availability Statement: Data sharing is not applicable to this article.

Acknowledgments: The authors would like to acknowledge the FOCAS Research Institute for providing research facilities.

Conflicts of Interest: The authors declare no conflict of interest.

References

1. Bunning, T.J.; Natarajan, L.V.; Tondiglia, V.P.; Sutherland, R.L. Holographic Polymer-Dispersed Liquid Crystals (H-PDLCs). *Annu. Rev. Mater. Sci.* **2000**, *30*, 83–115. [[CrossRef](#)]
2. Vita, F.; Lucchetta, D.E.; Castagna, R.; Criante, L.; Simoni, F. Effects of resin addition on holographic polymer dispersed liquid crystals. *J. Opt. A Pure Appl. Opt.* **2009**, *11*, 024021. [[CrossRef](#)]
3. Bigler, C.M.; Sarma, K.; Blanche, P.-A. Holographic waveguide heads-up display for longitudinal image magnification and pupil expansion. *Appl. Opt.* **2018**, *57*, 2007–2013. [[CrossRef](#)] [[PubMed](#)]
4. Duan, X.; Liu, J.; Shi, X.; Zhang, Z.; Xiao, J. Full-color see-through near-eye holographic display with 80° field of view and an expanded eye-box. *Opt. Express* **2020**, *28*, 31316–31329. [[CrossRef](#)] [[PubMed](#)]
5. Lee, Y.H.; Zhan, T.; Wu, S.T. Prospects and challenges in augmented reality displays. *Virtual Real. Intell. Hardw.* **2019**, *1*, 10–20. [[CrossRef](#)]
6. Keshri, S.; Murphy, K.; Toal, V.; Naydenova, I.; Martin, S. Development of a photopolymer holographic lens for collimation of light from a green light-emitting diode. *Appl. Opt.* **2018**, *57*, E163–E172. [[CrossRef](#)] [[PubMed](#)]
7. Park, J.; Cho, J.-Y.; Park, C.; Lee, K.; Lee, H.; Cho, Y.-H.; Park, Y. Scattering Optical Elements: Stand-Alone Optical Elements Exploiting Multiple Light Scattering. *ACS Nano* **2016**, *10*, 6871–6876. [[CrossRef](#)]
8. Marín-Sáez, J.; Atencia, J.; Chemisana, D.; Collados, M.-V. Characterization of volume holographic optical elements recorded in Bayfol HX photopolymer for solar photovoltaic applications. *Opt. Express* **2016**, *24*, A720–A730. [[CrossRef](#)]
9. Akbari, H.; Naydenova, I.; Ahmed, H.; McCormack, S.; Martin, S. Development and testing of low spatial frequency holographic concentrator elements for collection of solar energy. *Sol. Energy* **2017**, *155*, 103–109. [[CrossRef](#)]
10. Cheben, P.; Calvo, M.L. A photopolymerizable glass with diffraction efficiency near 100% for holographic storage. *Appl. Phys. Lett.* **2001**, *78*, 1490–1492. [[CrossRef](#)]
11. Carretero, L.; Murciano, A.; Blaya, S.; Ulibarrena, M.; Fimia, A. Acrylamide-N,N'-methylenebisacrylamide silica glass holographic recording material. *Opt. Express* **2004**, *12*, 1780–1787. [[CrossRef](#)] [[PubMed](#)]
12. Schnoes, M.G.; Dhar, L.; Schilling, M.L.; Patel, S.S.; Wiltzius, P. Photopolymer-filled nanoporous glass as a dimensionally stable holographic recording medium. *Opt. Lett.* **1999**, *24*, 658–660. [[CrossRef](#)]
13. Ramos, G.; Álvarez-Herrero, A.; Belenguer, T.; del Monte, F.; Levy, D. Shrinkage control in a photopolymerizable hybrid sol-gel material for holographic recording. *Appl. Opt.* **2004**, *43*, 4018–4024. [[CrossRef](#)] [[PubMed](#)]
14. Mikulchyk, T.; Oubaha, M.; Kaworek, A.; Duffy, B.; Lunzer, M.; Ovsianikov, A.; Sabad-E-Gul; Naydenova, I.; Cody, D. Synthesis of fast curing, water-resistant and photopolymerizable glass for recording of holographic structures by one- and two-photon lithography. *Adv. Opt. Mater.* **2022**, *10*, 2102089. [[CrossRef](#)]
15. Martínez-Matos, Ó.; Calvo, M.L.; Rodrigo, J.A.; Cheben, P.; del Monte, F. Diffusion study in tailored gratings recorded in photopolymer glass with high refractive index species. *Appl. Phys. Lett.* **2007**, *91*, 141115. [[CrossRef](#)]
16. Gómez-Romero, P.; Sanchez, C. *Functional Hybrid Materials*; Wiley-VCH: Weinheim, Germany, 2004; p. 417.
17. Phariseau, P. On the diffraction of light by progressive supersonic waves. *Proc. Indian Acad. Sci. Sect. A* **1956**, *44*, 165–170. [[CrossRef](#)]
18. Kogelnik, H. Coupled wave theory for thick hologram gratings. *Bell Syst. Tech. J.* **1969**, *48*, 2909–2947. [[CrossRef](#)]

19. Lee, K.C.; bin Saipolbahri, Z.A.; Soleimani, H.; Zaid, H.M.; Guan, B.H.; Ching, D.L.C. Effect of zinc oxide nanoparticle sizes on viscosity of nanofluid for application in enhanced oil recovery. *J. Nano Res.* **2016**, *38*, 36–39. [[CrossRef](#)]
20. Reiser, J.T.; Ryan, J.V.; Wall, N.A. Sol–gel synthesis and characterization of gels with compositions relevant to hydrated glass alteration layers. *ACS Omega* **2019**, *4*, 16257–16269.
21. Lee, T.Y.; Guymon, C.A.; Jönsson, E.S.; Hoyle, C.E. The effect of monomer structure on oxygen inhibition of (meth)acrylates photopolymerization. *Polymer* **2004**, *45*, 6155–6162. [[CrossRef](#)]
22. Hariharan, P. *Optical Holography: Principles, Techniques, and Applications*; Cambridge University Press: Cambridge, MA, USA, 1996; p. 428.
23. Versace, D.L.; Oubaha, M.; Copperwhite, R.; Croutxé-Barghorn, C.; MacCraith, B.D. Waveguide fabrication in UV-photocurable sol-gel materials: Influence of the photoinitiating system. *Thin Solid Films* **2008**, *516*, 6448–6457. [[CrossRef](#)]
24. Cullen, M.; O’Sullivan, M.; Kumar, A.M.; Sorour, A.A.; Duffy, B.; Oubaha, M. The role of the hydrolysis and zirconium concentration on the structure and anticorrosion performances of a hybrid silicate sol-gel coating. *J. Sol-Gel Sci. Technol.* **2018**, *86*, 553–567. [[CrossRef](#)]
25. Cerveau, G.; Corriu, R.J.P.; Framery, E. Nanostructured organic-inorganic hybrid materials: Kinetic control of the texture. *Chem. Mater.* **2001**, *13*, 3373–3388. [[CrossRef](#)]
26. Boury, B.; Corriu, R. Auto-organization in sol-gel type polycondensation: A door to the nanosciences. *Chem. Rec.* **2003**, *3*, 120–132. [[CrossRef](#)] [[PubMed](#)]
27. Bruder, F.-K.; Hansen, S.; Kleinschmidt, T.P.; Kunzel, R.; Manecke, C.; Orselli, E.; Rewitz, C.; Rolle, T. Integration of volume holographic optical elements (vHOE) made with Bayfol® HX into plastic optical parts. In *Proceedings of SPIE 10944: Practical Holography XXXIII: Displays, Materials, and Applications*; SPIE: Bellingham, WA, USA, 2019.